Research Article

For reprint orders, please contact: reprints@futuremedicine.com

Nanomedicine

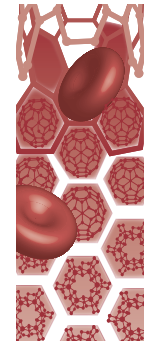

PLGA-encapsulated perfluorocarbon nanoparticles for simultaneous visualization of distinct cell populations by ^{19}F MRI

Mangala Srinivas*[,1], Jurjen Tel[1], Gerty Schreibelt[1], Fernando Bonetto[2], Luis-Javier Cruz[3], Houshang Amiri[4,5], Arend Heerschap[4], Carl G Figdor[1] & I Jolanda M de Vries[1]

[1]Department of Tumor Immunology, & Radboud University Medical Center, Radboud Institute for Molecular Life Sciences, Nijmegen, The Netherlands

[2]Instituto de Física del Litoral (CONICET – UNL), Santa Fe, Argentina

[3]Molecular Imaging, Leiden University Medical Center, Leiden, The Netherlands

[4]Department of Radiology, Radboud University Medical Center, Nijmegen, The Netherlands

[5]Neuroscience Research Center, Institute of Neuropharmacology, Kerman University of Medical Sciences, Kerman, Iran

*Author for correspondence:
Tel.: + 31 24 3617600
Fax: + 31 24 3540339
Mangala.Srinivas@radboudumc.nl

Aim: *In vivo* imaging using ^{19}F MRI is advantageous, due to its ability to quantify cell numbers, but is limited for a lack of suitable labels. Here, we formulate two stable and clinically applicable labels for tracking two populations of primary human dendritic cells (DCs) simultaneously. **Materials & methods:** Plasmacytoid and myeloid DCs are able to take up sufficient nanoparticles (200 nm) for imaging (10^{12} ^{19}F's per cell), despite being relatively nonphagocytic. **Results:** Clinically relevant numbers of labeled DCs could be imaged in about 10 min, even on a clinical scanner. **Conclusion:** We demonstrate the use of perfluorocarbon nanoparticles for simultaneous ^{19}F MRI of distinct cell populations in a clinical setting, without spectroscopic imaging.

Keywords: ^{19}F MRI • cell therapy • fluorescence • *in vivo* imaging • perfluorocarbons • PLGA

Cell tracking using noninvasive *in vivo* imaging techniques is a rapidly growing field, as it can contribute to the optimization of cellular therapeutics [1,2]. MRI has previously been used to monitor dendritic cell (DC) vaccines in melanoma patients using iron oxide contrast agents [3]. ^{19}F MRI is a relatively new imaging technique to be applied to cell tracking, and has several added advantages, chiefly, that it yields very specific images that allow for quantification of cell numbers without the use of radioactivity [4]. Nevertheless, a major problem with ^{19}F MRI for cell tracking has been the lack of stable, clinically applicable labels. The fluorous agents responsible for the detected signal – most often perfluorocarbons (PFCs) – are not miscible with hydrophilic or hydrophobic solvents, and thus can be difficult to stabilize in a form suitable for cell uptake [5]. Typically, emulsions are made using lipid surfactants and high-energy techniques such as microfluidization [6]. However, the poor affinity between the PFC, surfactant and aqueous continuous phase can limit emulsion stability. Furthermore, it can be difficult to add additional agents such as fluorescent dyes, drugs or antibodies without altering the emulsion properties, and with certainty of their localization within the emulsion. Recently, a commercial emulsion has been developed, although testing is still in the preliminary stages [7,8]. Approaching the issue of PFC stabilization in aqueous environments from a different angle, we developed polymer-encapsulated PFCs [9]. These particles have a modular structure where the particle content and coating can be tailored to the experimental system. A key advantage of using particles is that the components of the particles (fluorocarbon, dye or other encapsulated contents, surface coating or functionalization) can be modified without altering the formulation protocol. Furthermore, the particles can be lyophilized and stored as a stable powder. Finally, the particle components have all been previously used in humans (Figure 1A): PLGA has an extensive history of clinical use, Perfluorooctane (PFO) is available for clinical use in eye surgery (Perfluoron; Alcon Inc, USA) and perfluoro-15-crown ether (PFCE) has also recently been used in human volunteers [10]. Fluorescent dyes are available for human use (Fluorescite; Alcon Inc; and IC-Green; Akorn Inc, USA). Furthermore, we have found minimal effects on primary

Future Medicine part of fsg

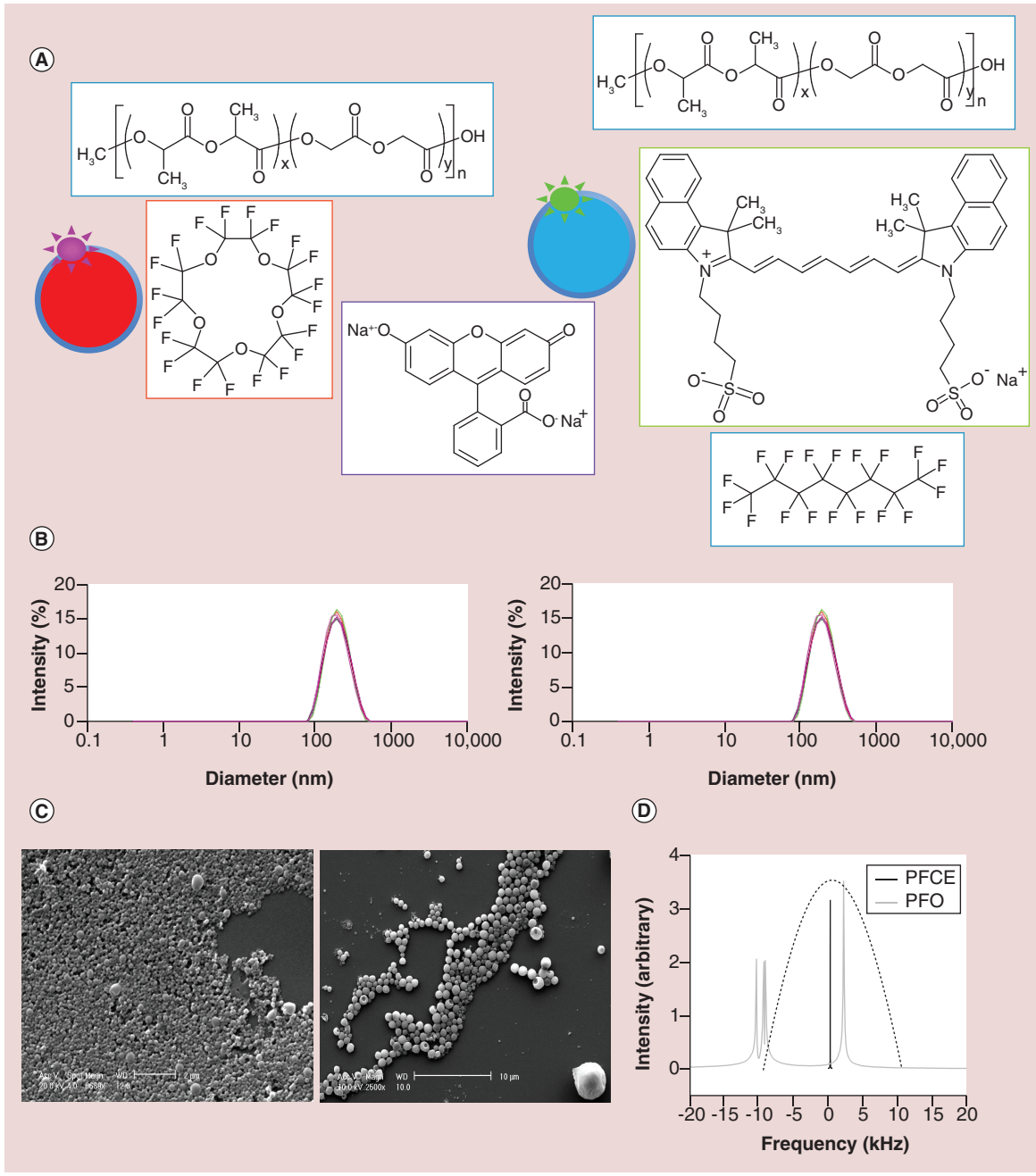

Figure 1. Particle composition and characteristics. (A) The particles consist of a perfluorocarbon encapsulated in PLGA, together with a fluorescent dye. Here, we combined either PFCE and IC-Green, or PFO and Flurorescite. **(B)** Representative diameter distribution of the PFCE, IC-Green (left) and PFO-Flurorescite particles are shown. The particles show a consistent and tight distribution. **(C)** Scanning electron micrographs of the PFCE, IC-Green particles show the spherical nature of the particles. Some particles display a depression. Scale bar represents 2 μm (left) and 10 μm (right). **(D)** The ^{19}F NMR spectrum, acquired at 7T, of both PFCE and PFO is shown. The curved line represents the excitation bandwidth used, which encompasses the PFCE peak and only the major peak of the PFO. PFCE: Perfluoro-15-crown ether; PFO: Perfluorooctane.

human monocyte-derived DCs after labeling with similar particles, in terms of viability and surface marker expression [9,11], and migration [12].

Cell tracking using ^{19}F MRI has been applied to various cell types, such as DCs, T cells and macrophages [6]. The next step in the application of ^{19}F MRI is the ability to track more than one cell population simultaneously. This is frequently done with other modalities, especially fluorescence imaging techniques. Recent work has also applied two different types of

MRI contrast agents, T_1 and T_2 agents, to tracking two cell populations in murine models [13]. Here, we exploit the particles and the technique to show the simultaneous imaging of two distinct therapeutic cell populations using different ^{19}F labels by synthesizing particles with distinct PFCs and fluorescent dyes. The use of distinct ^{19}F resonances has previously been proposed by us and other groups [11,14], using chemical shift imaging, but not standard imaging sequences. PFCs have also been emulsified with quantum dots to allow for spectrally selective ^{19}F MRI [15], where each PFC is imaged individually. However, here we show that both labeled cell populations can be imaged simultaneously using a gradient echo (GRE) sequence, resulting in much shorter imaging times, even on standard clinical scanners.

DCs are the main antigen-presenting cells of the immune system, and have the unique capacity to initate adaptive immune responses. This property is exploited in DC-based cancer immunotherapy (cell therapy), aimed at the specific activation of the immune system against cancer cells. Imaging plays a key role in the optimization of DC therapy, as these cells must migrate to lymph nodes to function properly [1]. Recent clinical evidence suggests that two specific subsets of circulatory DCs, plasmacytoid and myeloid DCs (pDCs and mDCs, respectively) may be potent cancer vaccines [16,17]. As pDC and mDC have complementary functions and can act synergistically for optimal immune responses [18], combination therapy using both cell types is thought to be beneficial [19]. A flaw in current DC therapy is the lack of insight in the *in vivo* behavior and mode of action of these cells. To monitor the *in vivo* biodistribution of pDC and mDC after DC vaccination, it is necessary to monitor both cell types individually in the same patient. In this paper, we formulate clinically applicable PLGA-encapsulated PFC particles for labeling these DC subsets, followed by simultaneous imaging on a clinical imaging system.

Materials & methods

Particle synthesis & characterization

PLGA-encapsulated PFC particles were synthesized as described [9]. Ninety milligrams of PLGA (Resomer RG 502 H, lactide: glycolide molar ratio 48:52 to 52:48; Boehringer Ingelheim, Ingelheim am Rhein, Germany; IUPAC name poly[DL-lactide-co-glycolide]) in dichloromethane was combined with 890 µl PFCE (Exfluor Inc, TX, USA; IUPAC name 2,2,3,3,5,5,6,6,8,8,9,9,11,11,12,12,14,14,15,15-icosafluoro-1,4,7,10,13-pentaoxacyclopentadecane) or 116 µl PFO (Perfluoron, Alcon Inc; IUPAC name 1,1,1,2,2,3,3,4,4,5,5,6,6,7,7,8,8,8-Octadecafluorooctane) and 1 mg IC-Green (Akorn Inc, USA; IUPAC name sodium 4-[2-[(1E,3E,5E,7Z)-7-[1,1-dimethyl-3-(4-sulfonatobutyl)benzo[e]indol-2-ylidene]hepta-1,3,5-trienyl]-1,1-dimethylbenzo[e]indol-3-ium-3-yl] butane-1-sulfonate) or 100 ug Fluorescite (Alcon Inc; IUPAC name 3′,6′-dihydroxyspiro[2-benzofuran-3,9′-xanthene]-1-one). This was added dropwise to an 80% poly-vinyl-alcohol solution under sonication with a cuphorn at 30% amplitude for 3 min in total (Digital Sonifier 250, Branson, Branson Sonic Power, CT, USA). This is then placed at 4 degrees with a magnetic stirrer for 18 h. The product is then centrifuged for 30 min at 21 × *g* at 4 degrees, and washed with purified water with two further centrifugation rounds. The suspension is then lyophilized for at least 24 h. Particles were made with either PFCE and IC-Green or PFO and Flurorescite. Dynamic light scattering was performed using a Malvern Zetasizer 2000 (Malvern, UK).

Imaging

MRI and spectroscopy was performed on a 7T MR system (Clinscan; Bruker Biospin, Ettlingen, Germany), equipped with a horizontal bore magnet (ultra shielded) and a gradient system with 20 cm inner diameter and maximum gradient strength of 300 mT/m. MRI was done on a 7T horizontal scanner, using a modified GRE sequence. False color ^{19}F images (TR/TE = 200/2.82 ms, 25° flip angle, 1.88 × 0.94 × 2 mm voxels, 256 averages, 12 min; bandwidth of 240 Hz/pixel) are overlaid on corresponding grayscale ^{1}H images (TR/TE = 1200/14 ms, 0.12 × 0.6 × 2 mm voxels, 1 average). Postprocessing was done to correct for the frequency shift using the known frequency of the label compounds and the bandwidth per pixel in the images. The bandwidth/voxel was noted, and thus the separation between the two resonances in the image was known. This was used to calculate the actual position of the received signal to create overlays, where the ^{19}F signals were each given a different color and superimposed over a grayscale ^{1}H image. For the *in vivo* image (5b), the mouse was anesthetized with isoflurane and imaged using a dual-tunable volume coil. A ^{1}H TSE was acquired (TR/TE = 2420/13 ms, 2 mm slices, 128 × 512 matrix, 1 average, FOV = 40 × 80 mm, acquisition time of 5.1 min). The ^{19}F image was acquired using a GRE sequence with TR/TE = 100/4.67 ms, 4 mm slices, 32 averages, flip angle of 25 degrees, 64 × 128 matrix, an FOV of 120 × 120 mm and an acquisition time of 1.7 min. Figure 2A was acquired on a Siemens 3T clinical scanner equipped with a Syngo workstation (version MR B17), using a custom-built dual tunable surface coil. A single tube containing 10 mg of both particles (10^{19} ^{19}F's each) dissolved in water was imaged. The ^{1}H image was acquired using a TSE, with TR/TE of 800/12 ms, FOV of 180 × 180 mm, matrix

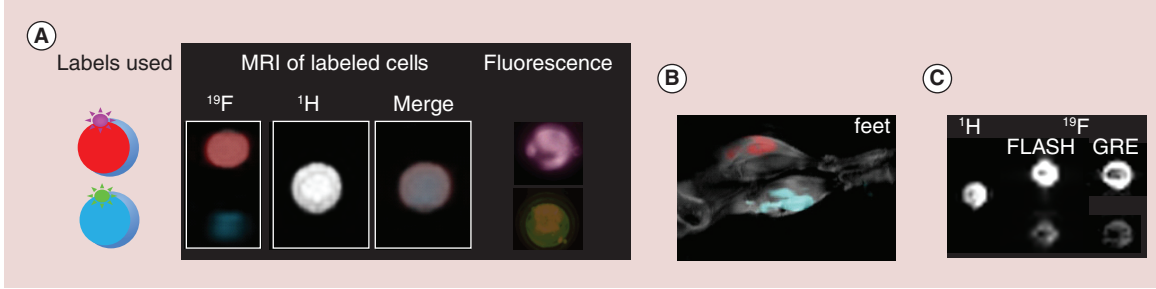

Figure 2. MRI and fluorescence 'two-color' images. (A) 0.5 million labeled plasmacytoid dendritic cells and 1 million labeled myeloid dendritic cells were placed in a tube and imaged using $^{1}H/^{19}F$ MRI and fluorescence. Both the raw ^{19}F image (with false color), and the processed image (corrected for chemical shift), are shown. **(B)** A mouse was injected intramuscularly with 5 mg of each particle, one in each leg. The processed ^{19}F image, overlaid on an anatomic ^{1}H image, is shown. This ^{19}F image was acquired in about 2 min. **(C)** A proof of principle image of both particles in a single tube imaged on a clinical scanner at 3T. The ^{19}F images are shown as acquired, with the perfluoro-15-crown ether above the perfluorooctane. The acquisition times for the FLASH and GRE scans were 3 and 1 min, respectively.

of 251 × 256 with slice thickness of 5 mm, a single average and an acquisition time of about 3 min. For the ^{19}F image, a FLASH sequence with a flip angle of 40 degrees, TR/TE of 200/9.8 ms, FOV of 70 × 70 mm, matrix of 80 × 80, 10 mm slice thickness, pixel bandwidth of 80 Hz and eight averages with an acquisition time of about 3 min. Alternatively, a ^{19}F GRE sequence was used, with TR/TE of 400/12.7 ms, FOV of 40 × 40, 40 degree flip angle, FOV of 40 × 40 mm, matrix of 80 × 80, 10 mm slice thickness, one average and an acquisition time of around 1 min.

Magnetic resonance spectrometry (MRS) was used to measure the ^{19}F content per cell. Labeled cell pellets were placed in sealed tubes with a reference sample of 100 µl of 0.5% solution of trifluoroacetic acid (TFA). The respective spectral weights was measured and compared with determine the ^{19}F content per cell. For fluorescence imaging, samples were placed in a FluorVivo 300 (INDEC BioSystems, CA USA). Exposure times were between 0.05 and 0.15 s. All regulatory guidelines were strictly followed for animal work.

Cells

Buffy coats (Sanquin, Nijmegen, The Netherlands) and patient material were obtained from volunteers after written informed consent and according to institutional guidelines. Peripheral blood mononuclear cells (PBMCs) were purified from buffy coats via ficoll density gradient centrifugation (Lymphoprep by Axis-Shield). To obtain peripheral blood leukocytes (PBLs), monocytes were depleted from PBMCs via adherence to plastic culture flasks. pDCs were purified from PBLs by positive isolation using anti-BDCA-4-conjugated magnetic microbeads (Miltenyi Biotec, Bergisch-Gladbach, Germany). $CD1c^+$ mDCs were purified from PBMCs by depletion of $CD19^+$ B cells followed by positive selection of $CD1c^+$ DCs using a $CD1c^+$ DC isolation kit (both Miltenyi Biotec, Bergisch-Gladbach, Germany). Cells were adjusted to 10^6 cells/ml in X-VIVO-15 (Lonza, Verviers, Belgium) supplemented with 2% of human serum. mDC and pDC purity was as assessed by flow cytometry on a FACS Calibur (BD Biosciences, NJ, USA) by double staining of $BDCA\text{-}2^+$-PE/$CD123^+$-FITC for pDCs and $CD11c^+$-PE/$CD1c^+$-APC for mDCs (Miltenyi Biotec). mDC and pDC purity was routinely up to 95% [20,21]. Plasmacytoid DCs were cultured overnight with 10 ng/ml rhIL-3 and PLGA-PFCE and mDCs were cultured overnight with 800 U/ml GM-CSF and PLGA-PFO. After overnight culture pDCs and mDCs were activated for 6 h in the presence of 4 µg/ml R848 (Axxora, Breda, The Netherlands).

Flow cytometry

Uptake of PLGA particles and the phenotype of mDCs and pDCs were determined by flow cytometry. Plasmacytoid DCs and mDCs were cultured overnight with different concentrations of PLGA particles containing PFC and atto-647. The following primary monoclonal antibodies (mAbs) and appropriate isotype controls were used: anti-BDCA2-PE, anti-CD123-APC, anti-CD11c-PE and anti-BDCA-1-APC (all Miltenyi Biotec); anti-HLA-ABC-PE, anti-HLA-DR/DP-FITC, anti-CD80-PE, anti-CD83PE, anti-CD86-APC (all BD Bioscience Pharmingen, CA, USA); anti-CD40-PE (Beckman Coulter, Mijdrecht, The Netherlands). Cells were analyzed by flow cytometry on a FACSCalibur (BD Biosciences, CA, USA).

Cytokine detection

Plasmacytoid DCs and mDCs were cultured overnight at a concentration of 10^5 DCs/100 µl/well in a 96-wells roundbottom plate. Supernatants were collected from DC cultures after 16 h of activation, and IFN-α (pDCs

only) and IL-6 production was analyzed by murine monoclonal capture and HRP-conjugated anti-IFNα antibodies (Bender MedSystems, Vienna, Austria) or anti-IL-6 Abs (Sanquin) using standard ELISA procedures. TNF-α was measured using a human Multiplex kit (Bender MedSystems) according to manufacturer's instructions.

Mixed lymphocyte reaction

Allogeneic peripheral blood lymphocytes (PBLs) were cocultured with differently matured pDCs and mDCs in a 96-well round bottom plate (DC:PBL ratio 1:20 with 1 × 10^5 PBL). After 4 days of culture, 1 µCi/well ([0.037 MBq]/well; MP Biomedicals, Amsterdam, The Netherlands) of tritiated thymidine was added for 8 h and incorporation was measured in a β-counter.

Transwell migration

For CCR7-mediated migration, a standard *in vitro* transwell migration assay was performed. 5 µm pore size polycarbonate membranes (Costar, London, UK) were placed upon an aliquot of 600 µl X-Vivo15 medium with 2% HS with or without chemokine (C-C motif) ligand 21 (CCL21) (100 ng/ml; Tebu-Bio). A total of 1 × 10^5 DCs in 100 µl culture medium were seeded in the upper compartment. Spontaneous migration was measured by incubation of the cells in a transwell without CCL21 in the lower compartment. DCs were allowed to migrate for 120 min in a 5% CO2, humidified incubator at 37°C. After incubation, beads (Beckman Coulter) were added to 600 µl culture medium containing migrated DCs and then counted by flow cytometry. All conditions were tested in duplicate.

Results

Particle synthesis and characterization

We synthesized different PLGA nanoparticles encapsulating PFCE, PFO, PFCE combined with the fluorescent dye IC-Green, or PFO combined with Fluorescite. The particle composition of the PFCE and PFO particles are summarized in Figure 1A. Particle size information is summarized in Table 1. The particles all show a tight distribution around 180 nm, regardless of the PFC or dye content. Particle diameter distributions are shown in Figure 1B (representative distributions shown). Electron micrographs of the PFCE particles (Figure 1C), show that the particles generally have a uniform spherical morphology; although some particles show a slight depression or dent. This has been observed in other constructs [22–24], and could arise from the peculiar properties of the PFC, suggesting a phase separation in the particles [25]. The formulation process can be carried out using standard lab equipment, and in a cleanroom environment for clinical use. Finally, Figure 1D shows the ^{19}F NMR spectra of PFCE and PFO. The imaging bandwidth was set to include the peak from the PFCE and the main peak from the PFO (dotted line). The remaining peaks from the PFO fall outside the bandwidth and were effectively ignored. The bandwidth central frequency is selected in the middle of both relevant peaks, so their intensities are equally affected by the resonance curve, assumed to be symmetrical around the central frequency.

Labeling of human pDCs & CD1c$^+$ mDCs

Freshly isolated human pDCs and mDCs were labeled by the addition of the particles to the medium. The survival and viability of blood DCs remained unaffected after the addition of PLGA particles (pDC viability 77 ± 5% [n = 3], mDC viability 82 ± 6% [n = 6]), even at high concentrations of 20 mg/ml/million cells, relative to nonlabeled cells. We optimized label concentrations initially by flow cytometry to detect fluorescence of the cells and subsequently by ^{19}F MRS (Figure 3A & B). This was necessary due to the limited numbers of cells, especially pDCs, that can be isolated from a single healthy donor. Flow cytometry needs much fewer cells than does NMR, and thus the testing was more extensive here. Based on the fluorescence analysis, maximal particle uptake occurred around 15 mg/ml for pDCs and 25 mg/ml for mDCs, which is comparable to the

Table 1. Summary of particle characteristics, namely content, diameter, polydispersity index and ^{19}F content. The particles show consistent diameters, low PDI and high ^{19}F loading. The ^{19}F loading is the total ^{19}F's for all resonances for the PFO particles. Standard deviation is indicated.

PFC	Dye	Diameter (nm)	PDI	^{19}F's/mg
–	–	187 ± 2	0.1	0
PFCE	–	176 ± 2	0.2	6 ± 1 × 10^{18}
PFCE	IC-Green	183 ± 2	0.1	5 ± 2 × 10^{18}
PFO	–	197 ± 5	0.2	3 ± 1 × 10^{18}
PFO	Fluorescite	184 ± 3	0.2	3 ± 0.8 × 10^{18}

PDI: Polydispersity index; PFC: Perfluorocarbon; PFCE: Perfluoro-15-crown ether; PFO: Perfluorooctane.

results obtained using MRS, which showed an average loading of 3 ± 0.5 × 10^{12} ^{19}F/pDC and 2 ± 0.3 × 10^{12} ^{19}F/mDC at these conditions. Note that we were not able to carry out ^{19}F NMR on pDCs labeled with different particle concentrations, as these cells are very rare (<0.1% of PBLs) and acquiring the necessary numbers of cells from a single healthy donor is not feasible. Furthermore, PFCE yields higher ^{19}F signal density than PFO, and this was chosen to label the pDCs. For all further experiments, pDC were labeled with 15 mg PLGA/1 × 10^6 pDC, mDC were labeled with 20 mg PGLA/1 × 10^6 mDC.

Effect of labeling on cells

Next we investigated whether the uptake of these PLGA particles affects the capacity of DCs to respond to TLR stimulation, a key natural function of the cells and important for efficient antigen presentation. Therefore, we studied the phenotype of freshly isolated DCs that were cultured overnight in the presence of PLGA particles and subsequently activated for 6 h with R848, a low-molecular-weight synthetic TLR7 and TLR8 agonist known to induce phenotypical maturation and secretion of proinflammatory cytokines by TLR7-expressing pDCs and TLR8-expressing mDCs [26]. The maturation status of pDCs and mDCs was studied by CD83 expression levels. Furthermore, expression of CD40, CD80, CD86, MHC class I and II was analyzed to determine the capacity to present antigen along with costimulation. In accordance with previous literature, culturing pDCs with IL-3 and mDCs with GM-CSF induced phenotypic maturation without the induction of cytokine secretion (Figure 4A & B) [27]. The addition of PLGA particles during culture affected neither the IL-3-induced pDC nor the GM-CSF-induced mDC phenotype (Figure 4A & B). Only the GM-CSF-induced expression levels of the common DC maturation marker CD83 on mDCs were elevated by the addition of the PLGA particles (Figure 4B). Importantly, after over-

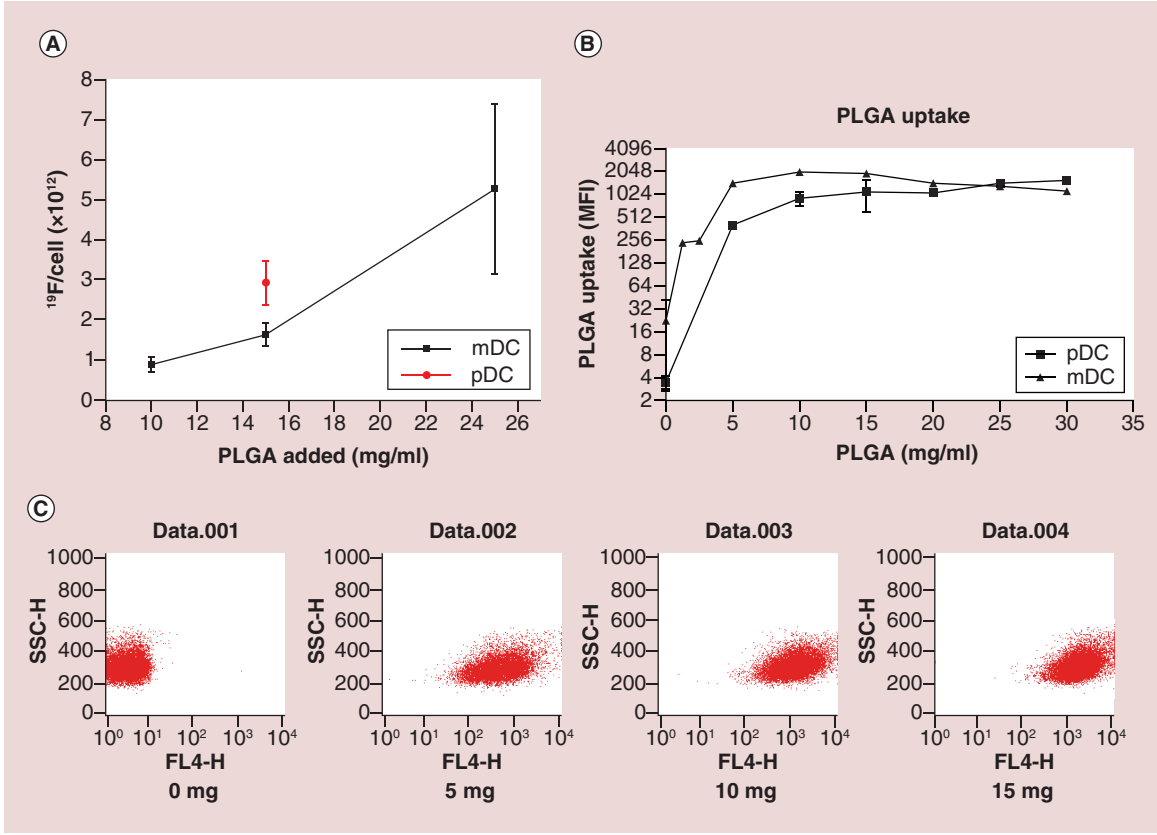

Figure 3. Cell labeling. (A) The ^{19}F loading of mDCs incubated with the indicated amounts of particles is shown, together with the loading of pDCs. Loading was in the order of 10^{12} ^{19}F's per cell for both cell types. **(B)** Particle uptake was measured more extensively using flow cytometry, where 0–30 mg of particles were added per million cells. Particle uptake appears to saturate around 10 mg for both cell types. Representative dot plots are shown, here for pDCs. **(C)** Flow cytometry data of labeled mDCs showing that the fluorescent particles were readily detected, and that fluorescence did not improve significantly beyond 10 mg of added particles under these conditions.
mDC: Myeloid dendritic cell; pDC: Plasmacytoid dendritic cell; PLGA: Poly(lactic-co-glycolic acid).

night culture with PLGA particles both blood DC types were still able to respond to TLR triggering by R848 as reflected by enhanced the expression levels of CD83 and the costimulatory molecule CD40, CD80 and CD86 (Figure 4A & B). Moreover, upon TLR triggering, both pDCs and mDCs secreted the inflammatory cytokines TNF-α and IL-6 (Figure 4C & D). Plasmacytoid DCs also secreted large quantities of IFN-α upon TLR7 ligation (Figure 4C). Interestingly, both pDCs and mDCs readily secreted TNF-α and IL-6 after uptake of PLGA particles, indicating that PFC containing particles provide stimulatory signals for cell activation (Figure 4C). Together, these data demonstrate that PLGA particles do not negatively affect DC phenotype or their ability to respond to TLR stimulation.

For effective immune responses, it is essential that activated DCs migrate to the T-cell areas of the draining lymph nodes to present antigen to naïve T cells. CCL21, the ligand for CCR7, is expressed by stromal and endothelial cells in the T-cell area of secondary lymphoid organs and is a major chemotactic attractant for DCs. In a Transwell migration assay, migration of pDCs and mDCs toward CCL21 was observed after 6 h of stimulation with R848, whereas no chemotactic activity was observed in the absence of CCL21 (Figure 4E & F). The addition of PFCs to the DC cultures slightly decreased pDC migration, whereas mDC migration was increased compared with nonlabeled DCs. PFC-labeled mDCs also showed increased migration in the absence of CCL21, suggesting higher migratory activity in general after PFC-labeling. However, both DC subsets still significantly migrated toward CCL21 after PFC treatment (Figure 4E & F). Thus, PLGA particle treatment followed by activation induces mature DCs with the capacity to migrate toward T-cell areas in the lymph node. This is a highly desirable outcome, as DC interaction with T cells is crucial to regulate the immune response.

Next, we studied the effect of labeling on the ability of the DCs to activate T cells, using a mixed lymphocyte reaction. DCs were harvested and cocultured with allogeneic PBLs, to induce T cell activation. After 4 days of coculture, proliferation was measured by ^{3}H-Thymidine incorporation. In accordance with previous findings [26], we found that both activated pDCs and mDCs have the capacity to evoke proliferative allogeneic T-cell responses (Figure 4G). Furthermore, we demonstrated that both labeled and 6 h activated pDCs as well as labeled and 6 h activated mDCs had an enhanced allostimulatory capacity compared with control cells as indicated by the proliferation of T cells (Figure 4G). Thus, the functionality, for example, migration, cytokine secretion and T cell stimulatory capacity, of blood DC subsets is warranted after the uptake of ^{19}F loaded biodegradable PLGA particles. This is in line with the results of other groups, which also show that uptake of particles can induce DC activation [28].

MR & fluorescence imaging

Identification of the two PFCs, and therefore the two cell populations, is based on the spectral separation of the PFCE peak and the relevant PFO peak, which is 2.4 kHz and results in a separation of 10 pixels in these images. This information was used to identify the signals acquired. Furthermore, the excitation pulse was set to a frequency between the relevant PFCE and PFO peaks, and was broad enough to excite both (Figure 1D). We detected all 20 ^{19}F atoms in PFCE as these all have a single resonance, but only a part of the ^{19}F signal from PFO (10 out of 16 total ^{19}Fs in the molecule). Figure 2A shows 1 million pDCs (false-colored in red) and 0.5 million mDCs (blue). The cell populations were mixed and placed in a single tube for imaging. Both the MR and fluorescence images are shown. Figure 2B shows a similarly processed image, where 5 mg of each particle were injected intramuscularly in each leg of a mouse. This is the equivalent of about a million labeled cells. Note that cells were not injected in the mouse, since we only labeled primary human cells and these would not be functional in mice. Here, the total imaging time was about 10 min. Figure 2C shows images of 10 mg particles acquired on a clinical scanner at 3T (equivalent of about 2 million labeled cells), using a clinical ^{19}F coil. A ^{19}F image was acquired in about 3 min, and an anatomical ^{1}H image in about 1 min.

Discussion

PLGA particles can be readily formulated with either PFC without any changes to the protocol. Furthermore, we have previously shown that PLGA–PFC particles are extremely stable [9]. The particles can also be tailored through the addition of drugs or other active agents [29,30]. We did not find any significant changes in particle diameter when the components (PFC and dye) were varied (Table 1). Cell loading is the highest reported when primary human monocyte-derived DCs are loaded with these particles [6]. Cell loading directly affects detection sensitivity, and is therefore a key parameter. Thus, we were able to load primary human pDCs and mDCs with sufficient amounts of the agent, without significant effects on the cells. Labeling nonphagocytic cells with emulsion-based agents often requires the use of transfection agents or other positively charged moieties, such as protamine sulfate, to improve cell loading [6]; these agents can

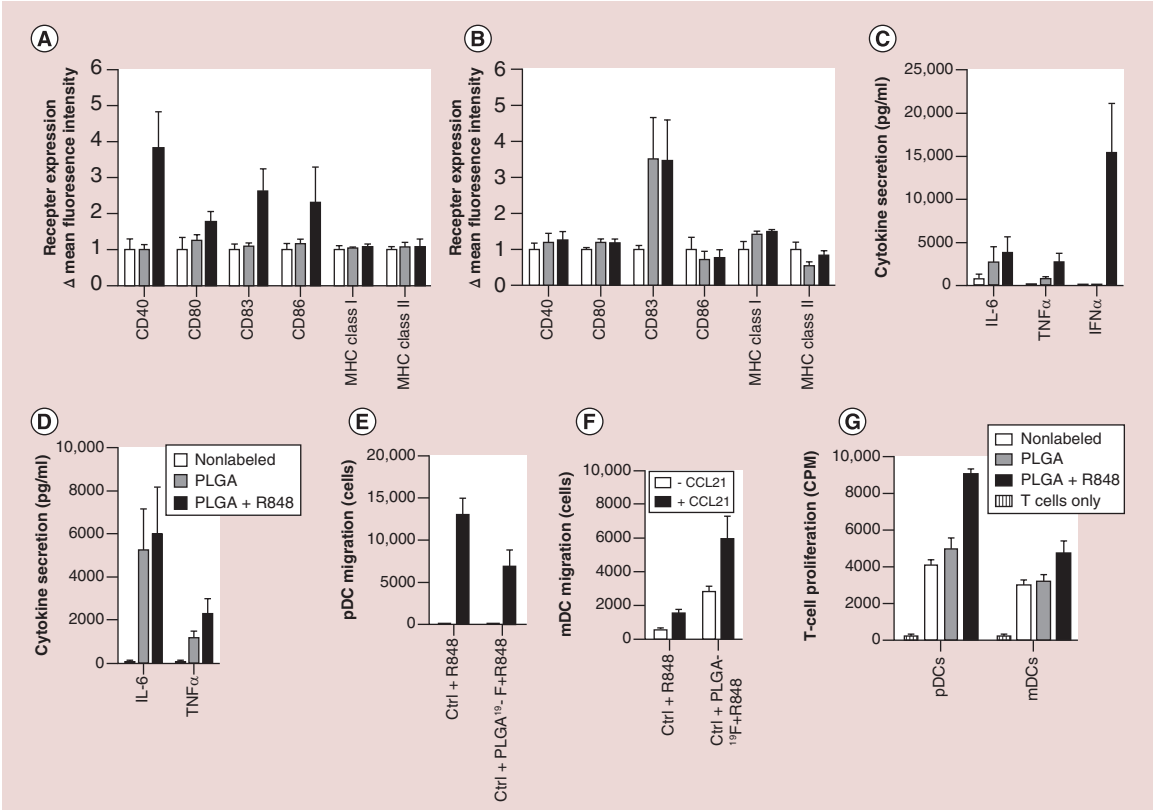

Figure 4. Effect of labeling on cells. No changes in surface marker expression upon maturation were observed upon labeling. Labeled cells could also secrete key cytokines upon R848 stimulation. Data are shown for pDCs **(A & C)** and mDCs **(B & D)**. Transwell migration assays for pDCs **(E)** and mDCs **(F)** show that the cells could migrate upon CCL21 stimulation. A slight increase in migration was observed even without stimulation with labeled mDCs. **(G)** Both mDCs and pDCs were able to induce T-cell division in a mixed leukocyte reaction.
mDC: Myeloid dendritic cell; pDC: Plasmacytoid dendritic cell; PLGA: Poly(lactic-co-glycolic acid).

reduce cell viability. The use of transfection agents was not necessary with the PLGA particles, even though the particles have a net negative zeta potential [9]. The reason behind this high uptake is unclear, although it could simply be that large amounts of particles can be added to the cells during incubation since the particles are not toxic, and this results in higher uptake, albeit at very poor efficiency (10% of added ^{19}F). One main concern was any possible effect of labeling on cell migratory ability, as this has been shown to be an issue with some MRI contrast agents [31]; however, this was not observed here (Figure 4E).

Lastly, the choice of PFCE and PFO allows the exploitation of their ^{19}F resonances for useful imaging, within the restrictions on clinical systems. Typically, multispectral imaging is carried out using peaks that are as far separated as possible, which is an advantage for spectroscopic sequences. However, our strategy allows for fast imaging, in place of traditional chemical shift imaging techniques, thus cutting imaging time significantly. We demonstrated imaging using a standard GRE and FLASH sequence, although it can be applied to any sequence with a sufficiently broad bandwidth. A disadvantage of the imaging technique, is that complex localization signals cannot be distinguished without some prior knowledge of distribution, or without the use of fluorescence to corroborate the data. However, in most cases, some prior knowledge of distribution is known and thus the technique remains largely applicable. There is also the possibility of ^{19}F MRS *ex vivo* on excised tissues to localize and quantify cells [32], which would result in higher sensitivity, as imaging time is not constrained *ex vivo*. Furthermore, the images shown (Figure 2), indicate that clinically relevant numbers of cells can be detected in a few minutes of imaging time, even using a standard 3T clinical scanner. This is in keeping with previous work using a similar set up which estimated an imaging time of less than a minute for 200,000 monocyte-derived DCs, where these cells are strongly phagocytic and take up at least tenfold more ^{19}F label [33].

Conclusion

The PLGA-encapsulated PFC particles described here can be used for the simultaneous imaging of distinct cell populations, with this combination of PFCs. The

particles can be used to label primary human DC subsets, even when the cells are relatively nonphagocytic. Importantly, cell functions such as migratory ability are not hindered by labeling. Furthermore, the imaging sequence applied here can readily be applied, even on clinical systems. Taken together, the imaging agents and sequence described in this paper allow for tracking more than one cell population simultaneously and efficiently.

Future perspective

^{19}F MRI is a quantitative imaging technique which does not suffer from depth penetration limits; however, it can be relatively slow and does not allow high resolution imaging. Fluorescence imaging allows for high resolution both in space and time, but is strongly restricted by penetration limits and bleaching of dyes. Thus, the two techniques complement each other beautifully. Moreover, ^{19}F MRI can be used in the clinic, while fluorescence could be used both for optimisation and later *in vitro* histology or analyses. Given the increasing popularity and complexity of cell therapies, we speculate that the ability to image different cell populations simultaneously using ^{19}F MRI, or even with spectroscopy, will become an increasingly popular technique.

Acknowledgements

The authors are grateful to Jeanette Pots, Olga Koshkina and Andor Veltien for assistance with the work.

Financial & competing interests disclosure

This work is funded by a Netherlands Organization for Scientific Research (NWO) VENI 700.10.409 and 86313024, NWO Spinoza award and NWO investment grants 91106021 and BIG (VISTA); European Research Council (ERC) ERC-2014-StG-336454-CoNQUeST and ERC-2010-AdG-269019-PATHFINDER; and The Netherlands Institute of Regenerative Medicine (NIRM, FES0908) and the EU FP7 program ENCITE (HEALTH-F5–2008–201842). The authors have no other relevant affiliations or financial involvement with any organization or entity with a financial interest in or financial conflict with the subject matter or materials discussed in the manuscript apart from those disclosed.

No writing assistance was utilized in the production of this manuscript.

Ethical conduct

The authors state that they have obtained appropriate institutional review board approval or have followed the principles outlined in the Declaration of Helsinki for all human or animal experimental investigations. In addition, for investigations involving human subjects, informed consent has been obtained from the participants involved.

Executive summary

- *In vivo* cell tracking can optimize cellular therapeutics; ^{19}F MRI is an imaging technique with several advantages, particularly quantification of cell numbers.
- Labels for ^{19}F MRI are difficult to formulate. Here, we show two distinct nanoparticles agents (200 nm diameter) with distinct ^{19}F resonances.
- Both types of nanoparticles can be imaged simultaneously using ^{19}F MRI, reducing imaging time.
- Primary human dendritic cell subsets, such as plasmacytoid and myeloid cells, can take up the agents in sufficient amounts.
- No significant effects were observed on the cells after labeling.
- Imaging on a clinical scanner with relevant cell numbers takes under 10 min, making it practically feasible.
- The nanoparticles can be customized, for example, by the addition of fluorescent dyes.
- The technique can eventually be applied to track different cell types simultaneously in the clinic upon cell transfer.

References

Papers of special note have been highlighted as:
• of interest; •• of considerable interest

1 Srinivas M, Aarntzen EH, Bulte JW *et al.* Imaging of cellular therapies. *Adv. Drug Deliv. Rev.* 62(11), 1080–1093 (2010).

•• **Reviews the role of imaging to optimize cell therapy.**

2 Ahrens ET, Bulte JW. Tracking immune cells *in vivo* using magnetic resonance imaging. *Nat. Rev. Immunol.* 13(10), 755–763 (1038) (2013).

• **Describes the different techniques for cell tracking using MRI.**

3 De Vries IJ, Lesterhuis WJ, Barentsz JO *et al.* Magnetic resonance tracking of dendritic cells in melanoma patients for monitoring of cellular therapy. *Nat. Biotechnol.* 23(11), 1407–1413 (2005).

• **The first published work using MRI for cell tracking in the clinic.**

4 Srinivas M, Heerschap A, Ahrens ET, Figdor CG, De Vries IJ. (^{19}) F MRI for quantitative *in vivo* cell tracking. *Trends Biotechnol.* 28(7), 363–370 (2010).

•• **Reviews the general pros and cons of ^{19}F MRI for cell tracking.**

5 Cametti M, Crousse B, Metrangolo P, Milani R, Resnati G. The fluorous effect in biomolecular applications. *Chem. Soc. Rev.* 41(1), 31–42 (2012).

6 Srinivas M, Boehm-Sturm P, Figdor CG, De Vries IJ, Hoehn M. Labeling cells for *in vivo* tracking using (^{19})F MRI. *Biomaterials* 33(34), 8830–8840 (2012).

7 Ahrens ET, Helfer BM, O'hanlon CF, Schirda C. Clinical cell therapy imaging using a perfluorocarbon tracer and

fluorine-[19] MRI. *Magn. Reson. Med.* 72 (6), 1696–1701 (2014).

8 Helfer BM, Balducci A, Nelson AD *et al.* Functional assessment of human dendritic cells labeled for *in vivo* ([19]) F magnetic resonance imaging cell tracking. *Cytotherapy* 12(2), 238–250 (2010).

9 Srinivas M, Cruz LJ, Bonetto F, Heerschap A, Figdor CG, De Vries IJ. Customizable, multi-functional fluorocarbon nanoparticles for quantitative *in vivo* imaging using [19]F MRI and optical imaging. *Biomaterials* 31(27), 7070–7077 (2010).

10 Hahn T, Kozerke S, Schwizer W, Fried M, Boesiger P, Steingoetter A. Visualization and quantification of intestinal transit and motor function by real-time tracking of [19] F labeled capsules in humans. *Magn. Reson. Med.* 66(3), 812–820 (2011).

11 Srinivas M, Cruz LJ, Bonetto F, Heerschap A, Figdor CG, De Vries IJ. Customizable, multi-functional fluorocarbon nanoparticles for quantitative *in vivo* imaging using [19]F MRI and optical imaging. *Biomaterials* 31(27), 7070–7077 (2010)

12 Bonetto F, Srinivas M, Weigelin B *et al.* A large-scale ([19]) F MRI-based cell migration assay to optimize cell therapy. *NMR Biomed.* 25(9), 1095–1103 (2012).

13 Di Corato R, Gazeau F, Le Visage C *et al.* High-resolution cellular MRI: gadolinium and iron oxide nanoparticles for in-depth dual-cell imaging of engineered tissue constructs. *ACS Nano* 7(9), 7500–7512 (2013).

14 Partlow KC, Chen J, Brant JA *et al.* [19] F magnetic resonance imaging for stem/progenitor cell tracking with multiple unique perfluorocarbon nanobeacons. *FASEB J.* 21(8), 1647–1654 (2007).

- **Describes the use of multiple [19]F resonances for cell tracking, but this could only be done using spectroscopic imaging.**

15 Lim YT, Noh YW, Cho JH *et al.* Multiplexed imaging of therapeutic cells with multispectrally encoded magnetofluorescent nanocomposite emulsions. *J. Am. Chem. Soc.* 131(47), 17145–17154 (2009).

16 Tel J, Aarntzen EH, Baba T *et al.* Natural human plasmacytoid dendritic cells induce antigen-specific T-cell responses in melanoma patients. *Cancer Res.* 73(3), 1063–1075 (2013).

17 Lou Y, Liu C, Kim GJ, Liu YJ, Hwu P, Wang G. Plasmacytoid dendritic cells synergize with myeloid dendritic cells in the induction of antigen-specific antitumor immune responses. *J. Immunol.* 178(3), 1534–1541 (2007).

18 Piccioli D, Sammicheli C, Tavarini S *et al.* Human plasmacytoid dendritic cells are unresponsive to bacterial stimulation and require a novel type of cooperation with myeloid dendritic cells for maturation. *Blood* 113(18), 4232–4239 (2009).

19 Bakdash G, Schreurs I, Schreibelt G, Tel J. Crosstalk between dendritic cell subsets and implications for dendritic cell-based anticancer immunotherapy. *Expert Rev. Clin. Immunol.* 10(7), 915–926 (2014).

- **Describes the synergy that develops when using multiple therapeutic cell subsets.**

20 Schreibelt G, Klinkenberg LJ, Cruz LJ *et al.* The C-type lectin receptor CLEC9A mediates antigen uptake and (cross-)presentation by human blood BDCA3+ myeloid dendritic cells. *Blood* 119(10), 2284–2292 (2012).

21 Tel J, Benitez-Ribas D, Hoosemans S *et al.* DEC-205 mediates antigen uptake and presentation by both resting and activated human plasmacytoid dendritic cells. *Eur. J. Immunol.* 41(4), 1014–1023 (2011).

22 Perro A, Reculusa S, Ravaine S, Bourgeat-Lami EB, Duguet E. Design and synthesis of Janus micro- and nanoparticles. *J. Mater. Chem.* 15(35–36), 3745–3760 (2005).

23 Martin-Banderas L, Duran-Lobato M, Munoz-Rubio I, Alvarez-Fuentes J, Fernandez-Arevalo M, Holgado MA. Functional PLGA NPs for oral drug delivery: recent strategies and developments. *Mini. Rev. Med. Chem.* 13(1), 58–69 (2013).

24 Ungaro F, D'angelo I, Miro A, La Rotonda MI, Quaglia F. Engineered PLGA nano- and micro-carriers for pulmonary delivery: challenges and promises. *J. Pharm. Pharmacol.* 64(9), 1217–1235 (2012).

25 Misra A, Urban MW. Acorn-shape polymeric nano-colloids: synthesis and self-assembled films. *Macromol. Rapid Comm.* 31(2), 119–127 (2010).

26 Tel J, Van Der Leun AM, Figdor CG, Torensma R, De Vries IJ. Harnessing human plasmacytoid dendritic cells as professional APCs. *Cancer Immunol. Immunother.* 61(8), 1279–1288 (2012).

27 Tel J, Torensma R, Figdor CG, De Vries IJ. IL-4 and IL-13 alter plasmacytoid dendritic cell responsiveness to CpG DNA and herpes simplex virus-1. *J. Invest. Dermatol.* 131(4), 900–906 (2011).

28 Rettig L, Haen SP, Bittermann AG *et al.* Particle size and activation threshold: a new dimension of danger signaling. *Blood* 115(22), 4533–4541 (2010).

29 Danhier F, Ansorena E, Silva JM, Coco R, Le Breton A, Preat V. PLGA-based nanoparticles: an overview of biomedical applications. *J. Control. Release* 161(2), 505–522 (2012).

30 Sah H, Thoma LA, Desu HR, Sah E, Wood GC. Concepts and practices used to develop functional PLGA-based nanoparticulate systems. *Int. J. Nanomedicine* 8, 747–765 (2013).

31 De Chickera SN, Snir J, Willert C *et al.* Labelling dendritic cells with SPIO has implications for their subsequent *in vivo* migration as assessed with cellular MRI. *Contrast Media Mol. Imaging* 6(4), 314–327 (2011).

32 Morel PA, Srinivas M, Turner MS *et al.* Gene expression analysis of dendritic cells that prevent diabetes in NOD mice: analysis of chemokines and costimulatory molecules. *J. Leukoc. Biol.* 90(3), 539–550

33 Bonetto F, Srinivas M, Heerschap A *et al.* A novel ([19]) F agent for detection and quantification of human dendritic cells using magnetic resonance imaging. *Int. J. Cancer* 129(2), 365–373 (2011).